


# Corneal Biomechanics Are Associated With *FBN1* Mutations in Patients With Marfan Syndrome and Ectopia Lentis

Qiu-Yi Huo,<sup>1-3</sup> Rui-Zheng Zhang,<sup>4</sup> Wan-Nan Jia,<sup>1-3</sup> Ya-Lei Wang,<sup>1-3</sup> Xin Shen,<sup>1-3</sup> Xin-Yao Chen,<sup>1-3</sup> Tian-Hui Chen,<sup>1-3</sup> Yan Liu,<sup>1-3</sup> Ling-Hao Song,<sup>1-3</sup> Xinyue Wang,<sup>1-3</sup> Yong Lv,<sup>5</sup> Ze-Xu Chen,<sup>1-3</sup> and Yong-Xiang Jiang<sup>1-3</sup> 

<sup>1</sup>Eye Institute and Department of Ophthalmology, Eye & ENT Hospital, Fudan University, Shanghai, China

<sup>2</sup>NHC Key Laboratory of Myopia (Fudan University), Key Laboratory of Myopia, Chinese Academy of Medical Sciences, Shanghai, China

<sup>3</sup>Shanghai Key Laboratory of Visual Impairment and Restoration, Shanghai, China

<sup>4</sup>Luoyang Central Hospital Affiliated To Zhengzhou University, Luoyang, China

<sup>5</sup>The First Affiliated Hospital of Zhengzhou University, Zhengzhou, China

Correspondence: Yong Lv, The First Affiliated Hospital of Zhengzhou University, Zhengzhou 450014, China;

[lyong@zzu.edu.cn](mailto:lyong@zzu.edu.cn).

Ze-Xu Chen, Department of Ophthalmology, Eye and ENT Hospital of Fudan University, Shanghai 200031, China; [Chenzexu430@163.com](mailto:Chenzexu430@163.com).

Yong-Xiang Jiang, Department of Ophthalmology, Eye and ENT Hospital of Fudan University, Shanghai 200031, China; [yongxiang\\_jiang@163.com](mailto:yongxiang_jiang@163.com).

QYH and RZZ contributed to this work equally.

**Received:** December 20, 2024

**Accepted:** February 13, 2025

**Published:** March 10, 2025

Citation: Huo QY, Zhang RZ, Jia WN, et al. Corneal biomechanics are associated with *FBN1* mutations in patients with marfan syndrome and ectopia lentis. *Invest Ophthalmol Vis Sci*. 2025;66(3):23. <https://doi.org/10.1167/iovs.66.3.23>

**BACKGROUND.** We investigated the corneal biomechanical properties and their genotype–phenotype correlation correlations in patients with Marfan syndrome (MFS) and ectopia lentis (EL).

**METHODS.** Patients with MFS with EL underwent panel-based next-generation sequencing in this retrospective cohort study. The *FBN1* genotypes were categorized into the dominant-negative (DN) group and the haploinsufficiency (HI) group. The DN variants were further subclassified based on the affected residues and their locations. Corneal biomechanical parameters were measured using dynamic Scheimpflug-based biomechanical analysis (CorVis ST). The correlations between corneal biomechanical properties and *FBN1* genotype or nongenetic factors were analyzed. The differences between patients with MFS and normal control were also evaluated after matching confounding factors.

**RESULTS.** One hundred one consecutive MFS probands participated in this study, with a median age of 6 years. Patients with HI and DN variants affecting critical residues, namely the DN (–Cys + CaB) variants, exhibited significantly higher deformation amplitude ratios ( $P = 0.029$ ) and lower stress–strain index values ( $P = 0.007$ ) compared with those in the DN (others) group, indicating lower corneal stiffness in the former group. DN variants in the FUN-EGF3 region were associated with lower deformation amplitude ratios ( $P = 0.011$ ) and higher stress–strain index values ( $P = 0.002$ ), whereas those in the DN–CD region exhibited the opposite pattern. Compromised corneal stiffness was significantly associated with HI and DN (–Cys + CaB) variants ( $b = -0.184$ ;  $P = 0.01$ ) and variants located outside the FUN-EGF3 region ( $b = 0.256$ ;  $P = 0.001$ ), after adjusting for confounding factors. Compared with matched controls, patients with MFS demonstrated significantly higher deformation amplitude ratios ( $P = 0.023$ ), further confirming decreased corneal stiffness in this population.

**CONCLUSIONS.** The *FBN1* genotype impacts the corneal biomechanical properties of patients with MFS and EL. Corneal biomechanics provide a novel platform to study the genotype–phenotype correlation of MFS.

**Keywords:** corneal biomechanics, *FBN1*, corneal visualization Scheimpflug technology, Marfan syndrome, ectopia lentis

Fibrillin microfibrils are expandable macromolecules that can serve as a structural scaffold for elastin deposition or form polymers alone, endowing connective tissue with elasticity and resilience in areas such as arteries, skin, zonules, and ligaments.<sup>1</sup> A spectrum of diseases resulting from a deficiency of fibrillin has been termed fibrillinopathies, with Marfan syndrome (MFS) being the most well-known.<sup>2</sup> MFS is caused by variants of the fibrillin 1 (*FBN1*) gene and presents

with varying manifestations in the cardiovascular, ocular, and musculoskeletal systems.<sup>3</sup> The mechanism behind the divergent phenotypes resulting from the same mutated gene remains largely elusive. Although growing evidence of genotype–phenotype correlations has been revealed in the cardiovascular system of MFS, little is known about these correlations in the ocular system, especially concerning properties other than ectopia lentis (EL).<sup>4</sup>

The cornea is the major refractive component of the eye, with its optical properties determined by both transparency and curvature. Experimental studies have confirmed the presence of both elastin-containing and elastin-free microfibril bundles in the corneal stroma, indicating a fundamental role of *FBN1* in providing elasticity and strength to the cornea.<sup>5,6</sup> Significant alterations in corneal biometry have been demonstrated in the eyes of patients with MFS, including a flatter curvature,<sup>7</sup> higher astigmatism,<sup>8</sup> increased light reflectivity,<sup>9</sup> and lower spherical aberration.<sup>10</sup> However, research into the biomechanical properties of the cornea has received less attention in this rare condition. With the advent of noncontact and dynamic corneal biomechanics devices, such as CorVis ST (Oculus Optikgeräte, Wetzlar, Germany),<sup>11</sup> the biomechanical properties of the cornea can now be obtained in vivo, offering opportunities to detect the effects of *FBN1* mutations on intact elastic tissue.

This study evaluates the corneal biomechanical parameters obtained by Corvis ST in patients with MFS, compares them with those of the normal population, and explores their correlation with the *FBN1* genotypes. We believe that the cornea has the potential to become a direct observational platform for broader biomechanics for MFS and related fibrillinopathies.

## METHODS

### Patient Eligibility

This study was approved by the Eye & ENT Hospital of Fudan University (ChiCTR2000039132) and conducted by the principles of the Declaration of Helsinki. Between 2021 and 2024, patients with MFS and EL were selected based on the following criteria: (1) diagnosis of EL via slit-lamp examination, (2) fulfillment of Ghent 2 nosology criteria for MFS or potential MFS,<sup>12</sup> (3) identification of a pathogenic or likely pathogenic *FBN1* mutation, and (4) availability of comprehensive clinical information. The exclusion criteria were (1) a history of ocular trauma or ocular surgery, (2) complex mutations involving multiple loci, (3) coexisting mutations associated with other ocular diseases, (4) poor cooperation with Corvis ST examination or failure to meet quality control standards, and (5) comorbidities such as retinal detachment, glaucoma, uveitis, or phthisis bulbi. Considering the binocular correlation, one eye was selected randomly for patients with bilateral EL. Only the proband of each pedigree was analyzed to minimize selection bias from family clustering. To avoid potential bias, the control group included healthy patients matched by age, sex, and axial length (AL) according to previous studies.<sup>13–16</sup>

### Ocular Examination

A thorough ophthalmic examination was conducted, including slit-lamp biomicroscopy, best-corrected visual acuity, and IOP measurement (Canon TX-20, Canon Medical Systems USA, Otawara, Tochigi, Japan). The severity of EL was quantified by measuring the angle between the pupil ring and lens ring under full pupillary dilation and classified as follows: severe ( $\alpha \geq 270^\circ$ ), moderate ( $180 < \alpha < 270^\circ$ ), and mild ( $\alpha \leq 180^\circ$ ).<sup>17</sup> Ocular biometric parameters were obtained using partial coherence interferometry (IOLMaster 700, Carl Zeiss Meditec AG, Jena, Germany), including anterior chamber depth, AL, lens thickness, keratometry (K) in both the flat (K1) and steep K (K2), corneal astigmatism, and white-to-

white. The corneal biomechanical properties were captured using a dynamic high-speed Scheimpflug camera (CorVis ST) and analyzed in conjunction with geometric topography obtained by Pentacam (Oculus Optikgeräte GmbH, Wetzlar, Germany).

The corneal biomechanical parameters were broadly classified into three categories. (1) The first category includes common CorVis ST indicators: the time of the first and to the second applanation (A1T and A2T), the length of the flattened segment in the first applanations and the second applanation (A1L and A2L), velocity of corneal movement during the two applanations (A1V and A2V), peak distance (PD) at the highest concavity, and deformation amplitude at the highest concavity (deformation amplitude [DA]). (2) The second category comprises compound biomechanical screening parameters, which are derived from the previously mentioned indicators: stiffness parameter at the first applanation (SP A1), integrated radius (IR), Ambrósio's relational thickness horizontal (ARTh), DA ratio max (2 mm), and stress-strain index (SSI). (3) The third category includes corneal ectasia indicators, such as the Belin/Ambrósio deviation (BAD D), Corvis Biomechanical Index, and tomographic biomechanical index (TBI). The definitions of these corneal biomechanical indicators are detailed in Supplementary Table S6. Additionally, certain morphological parameters indicative of corneal ectasia obtained via Pentacam were also included, such as K max, inferior minus superior value, and Pentacam random Forest index.

### Genotyping Process

Peripheral venous blood was collected from all participants. The sequenced DNA libraries underwent enrichment using an EL-specific panel-based next-generation sequencing, developed in collaboration with Amplicon Gene (Shanghai, China) using the Illumina Novaseq 6000 (Illumina, San Diego, CA, USA) platform.<sup>17</sup> The customized NGS panel of 41 genes for MFS and congenital EL is shown in Supplementary Table S1. The Ensembl Variant Effect Predictor 105, an integrated in silico tool, was used to predict splicing sites, annotate allele frequencies, and assess the pathogenicity of missense variants, using the reference sequence NM\_000138.5. Candidate variants were confirmed through Sanger sequencing, which also facilitated genotype-phenotype co-segregation analysis among family members. For patients suspected of MFS in whom no likely pathogenic variant was detected, multiplex ligation-dependent probe amplification was conducted as a supplementary analysis. All mutations were evaluated according to the guidelines of the American College of Medical Genetics and Genomics<sup>18</sup> and the *FBN1*-specific criteria outlined in the revised Ghent nosology.<sup>12</sup>

We classified *FBN1* mutations into two main groups: dominant negative (DN) and haploinsufficiency (HI). The DN group included missense variants and in-frame deletions or insertions, while the HI group encompassed frameshift variants, nonsense variants, splicing variants, and intra-genic deletions or duplications. The DN variants were further subclassified based on their impact on specific residues. Missense variants affecting key structures, such as cysteine residues involved in disulfide bridge formation and conserved motifs crucial for calcium binding in cb epidermal growth factor-like domains, were categorized as DN (–Cys + CaB). Variants not affecting these critical residues were clas-

sified as DN (others).<sup>17</sup> Additionally, DN variants were classified according to their exon locations: the N-terminal region (exons 1–21), a C-terminal region (exons 43–65), and the middle region (exons 22–42).<sup>19</sup> Specific functional regions or previously reported regions were also analyzed, including the FUN-EGF3 region (exons 1–11), neonatal region (exons 24–32), TGF- $\beta$  regulatory sequence (exons 43–65), and DN-CD region (exons 25–36 and 43–49), were also explored.<sup>17</sup> The DN mutations were also categorized according to their location in the protein domain referring to the UMD-*FBN1* database (<http://umd.be/FBN1/>).

## Statistical Analysis

The distribution of continuous parameters was assessed for normality using the Shapiro-Wilk test. Demographic data were presented as mean  $\pm$  standard deviation for continuous variables with a normal distribution, as median (interquartile range) for continuous variables without normal distribution, and as frequencies (%) for categorical variables. Comparisons of corneal biomechanical indicators among

different genotype groups were conducted using the Student *t* test, one-way ANOVA, Mann-Whitney *U* test, or Kruskal-Wallis test, as appropriate. Pearson's or Spearman's correlation was calculated to evaluate the relationships between ocular biometric characteristics and corneal biomechanical indicators. Variables with a *P* value of less than 0.10 in univariate analysis or those with clinical relevance were included in the multivariate analysis. The MFS group was matched to the control group for potential confounding factors. Statistical analyses were performed using SPSS version 27.0 software (SPSS Inc., Chicago, IL, USA), with a two-sided *P* value of less than 0.05 considered statistically significant.

## RESULTS

### Demographic Profile

A summary of the study workflow is illustrated in Figure 1. A total of 101 patients with MFS and EL were recruited, with a median age of 6.00 years (interquartile range,

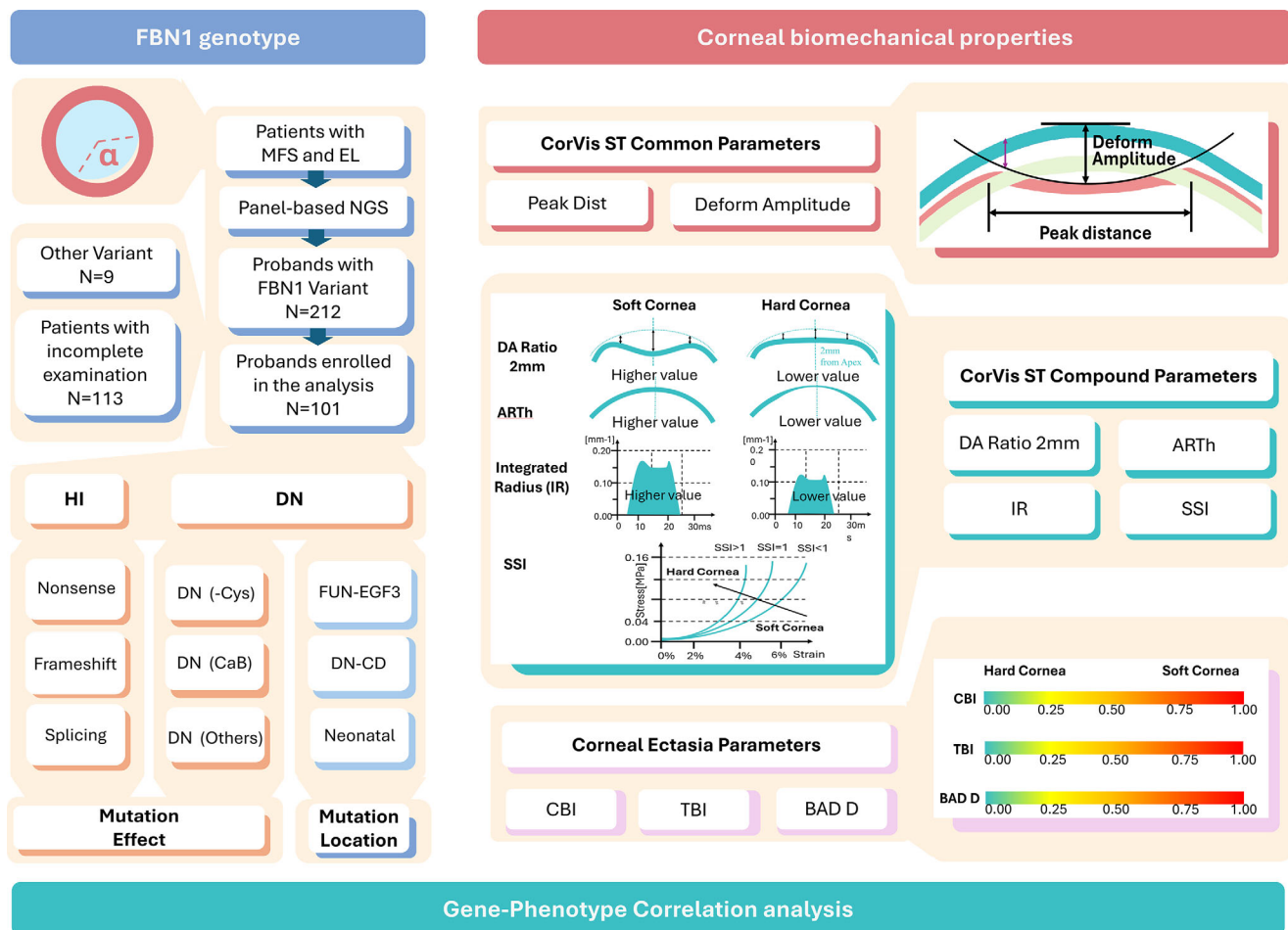


**FIGURE 1.** Schematic diagram of the workflow. This project is structured into three stages. In the first stage, we enrolled patients with MFS and EL who had confirmed *FBN1* variants and comprehensive clinical profiles. The *FBN1* genotypes were categorized based on mutation effects and locations. In the second stage, corneal biomechanical data were collected using CorVis ST technology, with the indicators classified into three groups: common, compound, and corneal expansion indicators. Finally, we analyzed the correlation between corneal biomechanical properties and *FBN1* genotype, and adjusted potential confounding factors. CBI, Corvis Biomechanical Index; DN (-Cys), DN variants eliminating the disulfide-bridge forming cysteines; DN (CaB), DN variants affecting the conserved calcium-binding motif; DN (others), DN variants affecting other residues; SSI, stress-strain index.

TABLE. Demographic and Ocular Characteristics

Characteristics	Mean $\pm$ SD, Median (IQR), or No. (%)
Demographic characteristics	
Age, years	6.00 (4.00 to 14.50)
Female sex	45 (44.6%)
Ocular biometric parameters	
Right eye	57 (56.4%)
AL (mm)	23.54 (22.67 to 25.47)
IOP (mmHg)	16.50 (15.00 to 18.15)
ACD (mm)	3.31 (3.01 to 3.58)
K1 (D)	40.11 $\pm$ 1.65
K2 (D)	41.96 (40.53 to 42.94)
Cyl (D)	-1.70 (-2.28 to -1.14)
LT (mm)	3.86 (3.62 to 4.34)
CCT (mm)	544.53 $\pm$ 43.55
WTW (mm)	12.15 $\pm$ 0.53
CorVis ST common indicators	
PD (mm)	4.82 $\pm$ 0.43
Radius (mm)	6.61 (5.89 to 7.52)
Deform Amplitude (mm)	1.00 (0.92 to 1.09)
CorVis ST compound parameters	
SP A1	108.07 $\pm$ 23.05
IR (mm <sup>-1</sup> )	8.48 $\pm$ 1.41
ARTh	550.20 (484.15 to 667.40)
DA Ratio (in 2 mm)	4.11 $\pm$ 0.42
SSI	0.93 (0.78 to 1.07)
Corneal ectasia parameters	
CBI	0.10 (0.04 to 0.34)
TBI	0.35 (0.13 to 0.56)
BAD D	0.68 $\pm$ 0.82
Morphological parameters indicating corneal ectasia	
K Max(D)	42.26 $\pm$ 1.73
I-S Value	0.35 $\pm$ 0.83
PRFI	0.14 (0.07 to 0.30)

ACD, anterior chamber depth; ARTh, Ambrosio rational thickness horizontal; BAD D, Belin/Ambrosio index; CBI, Corvis Biomechanical Index; Cyl, corneal astigmatism; I-S value, inferior-superior value; K Max, maximal keratometry; K1, flat K; K2, steep K; LT, lens thickness; PD, peak distance; PRFI, Pentacam random Forest index; SP A1, stiffness parameter A1; SSI, stress-strain index; TBI, tomographic biomechanical index; WTW, white to white.

4.00–14.50 years) at the time of examination (Supplementary Table S2). The distribution of ocular biometric and biomechanical parameters is detailed in Table. Approximately 80% of the *FBN1* variants were missense mutations, with a tendency to cluster in the N-terminal region (Fig. 2A). Among the DN variants, the highest proportion was DN (–Cys), followed by DN (others) and DN (CaB) (Fig. 2B, Supplementary Table S5).

### The Correlation Between Corneal Biomechanical Properties and Genotype

Corneal biomechanical parameters were analyzed across different genotype categories. Patients in the DN group and HI group manifested similar corneal biomechanical properties (Supplementary Table S3). When the DN variants were subdivided, patients with HI or DN (–Cys + CaB) variants showed significantly higher DA Ratio ( $P = 0.029$ ) and lower SSI ( $P = 0.007$ ) compared with those in the DN (others) group (Fig. 3A). In the genotype classification based on vari-

ant location, the DA Ratio was significantly higher in patients with variants in the DN–CD region ( $P = 0.021$ ), but lower in those with variants in the FUN–EGF3 region ( $P = 0.011$ ). Conversely, the SSI value was lower in the DN–CD region group ( $P = 0.018$ ), but higher in the FUN–EGF3 region group ( $P = 0.002$ ). Additionally, patients with variants in the DN–CD region had significantly larger PD ( $P = 0.014$ ), although the difference was insignificant in the other two groups (Fig. 3A).

### The Correlation Between Corneal Biomechanical and Biometrical Parameters

The relationship between corneal biomechanical properties and other factors was also investigated (Fig. 3B). Generally, most corneal biomechanical parameters were influenced by sex, age, IOP, AL, K, and central corneal thickness (CCT). Males exhibited higher ARTh and BAD D compared with females but had lower Corvis Biomechanical Index values. Age showed a negative correlation with the TBI, SSI, and IR, and positively correlated with SP A1. IOP was correlated negatively with IR and DA ratio but positively correlated with SP A1. AL was negatively correlated with TBI, SSI, and IR. CCT was associated with most factors, except for SSI and inferior-superior value. Additionally, K2 was found to correlate with more biomechanical parameters than K1. Furthermore, white-to-white was negatively correlated with BAD D and positively correlated with ARTh. The severity of EL did not significantly affect corneal biomechanical properties (Fig. 3B).

### Multivariate Analysis

Given that both genetic and demographic characteristics influence corneal biomechanical parameters, multivariate analysis was conducted for the DA Ratio (Fig. 4), SSI (Supplementary Fig. S1), and inferior-superior value (Supplementary Fig. S2). K2 was included in the multivariate regression model owing to its strong correlation with various biomechanical parameters. The HI + DN (Cys + CaB) genotype ( $b = -0.184$ ;  $P = 0.01$ ), K2 ( $b = 0.076$ ;  $P < 0.001$ ), IOP ( $b = -0.065$ ;  $P < 0.001$ ), and CCT ( $b = -0.003$ ;  $P < 0.001$ ) were significantly correlated with the DA Ratio. The FUN–EGF3 region genotype ( $b = -0.256$ ;  $P = 0.001$ ), IOP ( $b = -0.056$ ;  $P < 0.001$ ), and CCT ( $b = -0.005$ ;  $P < 0.001$ ) were also significantly correlated with the DA ratio. Additionally, within the DN–CD region group, IOP ( $b = -0.053$ ;  $P < 0.001$ ) and CCT ( $b = -0.005$ ;  $P < 0.001$ ) continued to affect the DA Ratio (Fig. 4) significantly.

### Comparison With Matched Controls

To determine whether the observed genotype-phenotype correlations in patients with MFS represent distinct features or broader variations within the general population, we compared the corneal biomechanical properties of the MFS group with those of a normal control group. After matching for age, gender, and AL, a subset of 29 patients with MFS and 27 healthy controls were included in the analysis (Supplementary Table S4). The patients with MFS manifested significantly lower SP\_A1 ( $P = 0.03$ ), lower ARTh ( $P = 0.017$ ), and higher DA ratio ( $P = 0.023$ ) compared with the normal controls.



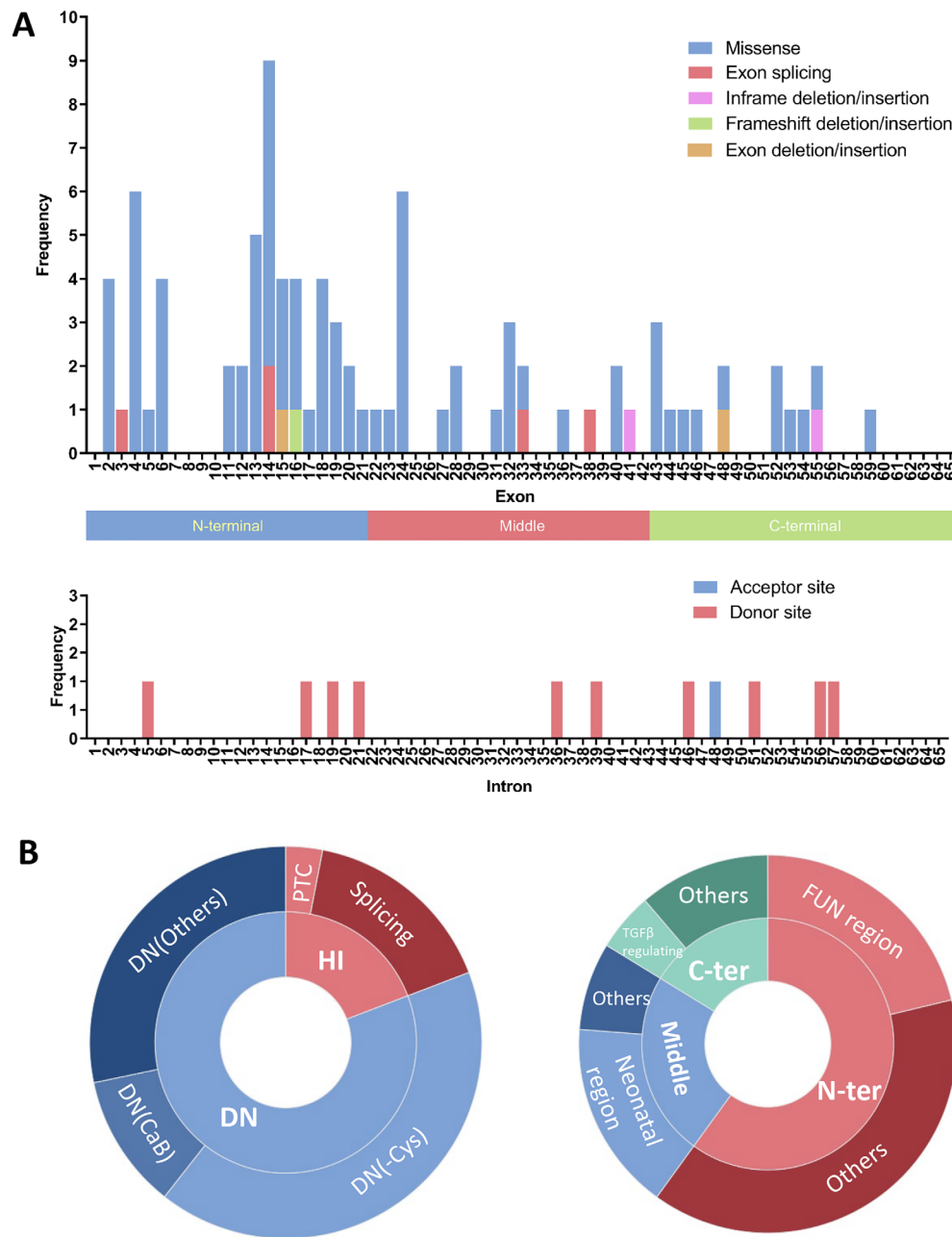


**FIGURE 2.** Genetic spectrum of the MFS cohort. **(A)** Frequency of *FBN1* mutations per exon (upper panel) and intron (lower panel). Mutations are mapped to the corresponding regions: N-terminal (exons 1–21), middle (exons 22–42), and C-terminal (exons 43–65). **(B)** Distribution of genotype subgroups classified by mutation effect (*left*) and location (*bottom*). The HI subgroup includes PTC and splicing mutations. The DN subgroup is further subdivided into DN (CaB), DN (–Cys), and DN (Others) based on the affected residue. DN variants are also categorized by their location in the N-terminal, middle, and C-terminal regions, with specific focus on the FUN-EGF3 region (exons 1–11), neonatal region (exons 24–32), and TGF- $\beta$  regulatory sequence (exons 43–65). DN, dominant negative; DN (–Cys), DN variants eliminating the disulfide-bridge forming cysteines; DN (CaB), DN variants affecting the conserved calcium-binding motif; DN (others), DN variants affecting other residues; EGF, epidermal growth factor; PTC, premature termination codon.

## DISCUSSION

With the advancement of in vivo biomechanics measurement instruments, the biomechanical properties of the cornea have been investigated in both normal and pathological conditions. As a biological tissue, the cornea exhibits characteristic mechanical properties that are essential for maintaining its curvature and resisting external forces.<sup>20</sup> Alterations in these biomechanical properties not only assist

in diagnosing corneal deformities, but also provide fundamental insights into the underlying pathogenesis.<sup>21</sup> In this study, we used a dynamic high-speed Scheimpflug camera, the CorVis ST, to assess the corneal biomechanical properties in patients with MFS, to compare them with healthy controls, and to explore their correlation with the *FBN1* genotype. This approach offers novel insights into the physiological role of *FBN1* in the cornea and the effects of its mutations.

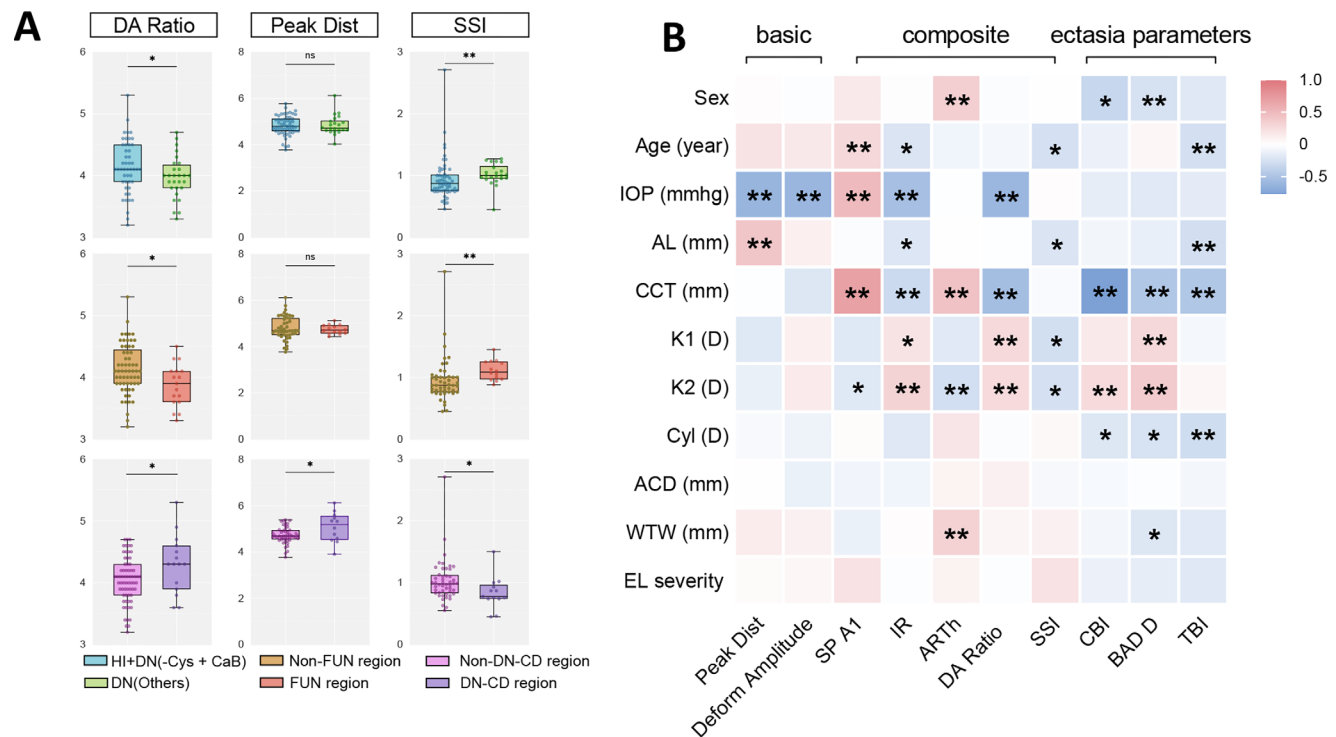


**FIGURE 3.** Influencing factors of ocular biomechanical properties. **(A)** Comparison of DA Ratio, PD, and SSI among *FBN1* genotype subgroups. Statistical significance is indicated with asterisks: \* $P < 0.05$ , \*\* $P < 0.01$ . **(B)** Correlation analysis between corneal biomechanical properties and nongenetic factors. Significant correlations are denoted with asterisks: \* $P < 0.05$ , \*\* $P < 0.01$ . ACD, anterior chamber depth; CBI, Corvis Biomechanical Index; Cyl, corneal astigmatism; DA ratio, deflection amplitude ratio; LT, lens thickness; SP-A1, stiffness parameter A1.

In addition to the cardinal ocular feature of EL, the cornea in MFS has been observed to be flatter, thinner, and exhibiting higher astigmatism compared with the general population.<sup>22</sup> Ultrastructural studies in *Fbn1*-deficient mice have revealed a significantly reduced density, disorganized micro fibrillin bundles, increased spacing between collagen fibers, and decreased glycosylated protein aggregation in the corneas.<sup>23</sup> However, these characteristics, although statistically significant among patients with MFS, have limited diagnostic value owing to substantial individual variability. Previous research has indicated that approximately 25% of patients with MFS have a K value exceeding 42 D,<sup>7</sup> and approximately 40% of them have a CCT of  $>500 \mu\text{m}$ .<sup>24</sup> Although our study demonstrated compromised corneal stiffness in patients with MFS, the literature on corneal biomechanical changes in patients with MFS remains inconsistent. Beene et al.<sup>14</sup> reported reduced resistance of the cornea to bending in patients with MFS, whereas Jin et al.<sup>13</sup> found the opposite; Kara et al.<sup>25</sup> observed no significant differences between patients with MFS and matched controls. These discrepancies may stem from the allelic heterogeneity of *FBN1*. Previous studies have shown that the *FBN1* genotype can impact the EL severity,<sup>26</sup> CCT,<sup>27</sup> AL,<sup>26</sup> and its growth rate among patients with MFS.<sup>17</sup> However, the correlation between the *FBN1* genotype and corneal biomechanical properties remained unexplored. This study identified several genotype clusters with significantly different corneal biomechanical properties, reinforcing the hypothesis that the corneal features in MFS are influenced by the varying effects of *FBN1* mutations.

Based on their effects, *FBN1* variants can be broadly categorized into HI variants with decreased expression and DN variants having a normal expression but compromised structure. Previous studies have indicated that HI variants are linked to a higher risk of aortic dilation and a shortened lifespan compared with DN variants.<sup>28</sup> When subclassifying DN variants based on the residues affected, DN (–Cys + CaB) variants, which impact critical disulfide-bond-forming cysteines and the conserved calcium-binding motifs in the tandem cb epidermal growth factor-like domains, have been shown to correlate with more severe MFS.<sup>29</sup> Some studies also extract the DN (–Cys) variants from the DN group and combine them with HI variants when assessing aortic risk in patients with MFS.<sup>30</sup> Consequently, in this study, we grouped HI variants and DN (–Cys + CaB) variants together, potentially representing a more severe MFS cluster. Patients with these *FBN1* variants exhibited significantly lower SSI but higher DA Ratio compared with those with the DN (others) variants, indicating the more severely compromised cornea stiffness in the former group. This finding aligns with previous research suggesting that the corneas of patients with MFS with higher systemic scores exhibited reduced resistance to external stimuli.<sup>15</sup> Meanwhile, a prior study showed that *FBN1* variants in the DN–CD region are associated with larger aortic root Z-scores and a higher risk of aortic events.<sup>28</sup> This study also revealed that the variants in this region correlated with a higher PD, lower SSI, and higher DA ratio, although these correlations did not persist in multivariate analysis. Furthermore, variants in the FUN–EGF3 region, a newly defined region critical for the end-to-end assembly of *FBN1* located at its extreme N-terminus,<sup>31</sup> were asso-

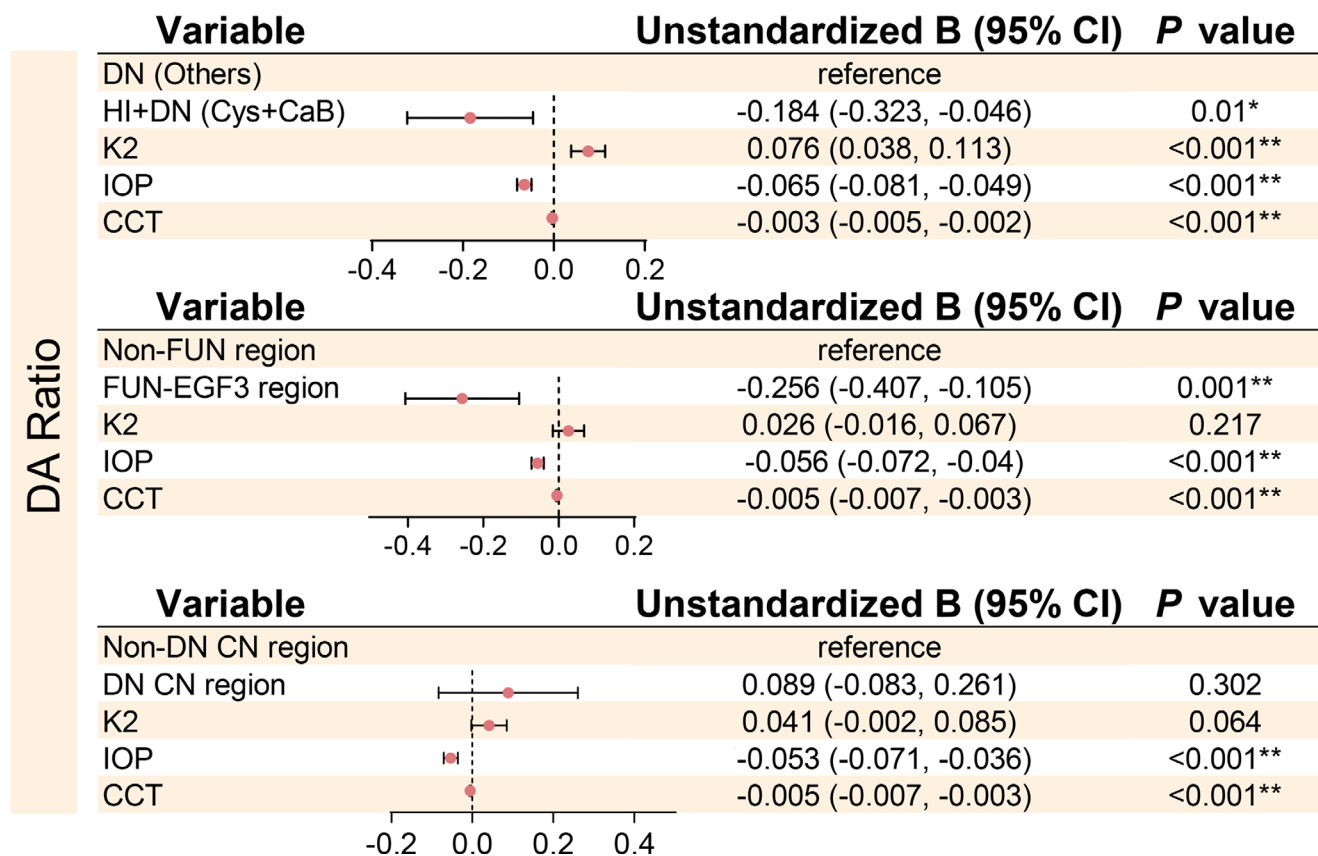


**FIGURE 4.** Multivariate analysis of DA ratio. Forest plot illustrating the multivariate analysis of the DA Ratio. The analysis revealed significant associations between DA Ratio and the *FBN1* genotype within the HI+DN(–Cys+CaB) and FUN-EGF3 region groups. Additionally, IOP and CCT were identified as significant factors influencing the DA ratio. Asterisks denote statistical significance: \* $P < 0.05$ , \*\* $P < 0.01$ . CCT, central corneal thickness; DN (–Cys+ CaB), DN variants eliminating the disulfide bridge-forming cysteines or affecting the conserved calcium-binding motif; K2, steep meridian.

ciated with increased corneal stiffness even after adjusting for nongenetic characteristics. This observation supports the notion that *FBN1* variants in the extreme terminus are linked to milder and atypical phenotypes.<sup>3</sup> Our study demonstrated reduced corneal stiffness in patients with MFS and suggested a correlation with more severe *FBN1* mutations. Given this genetic basis, corneal biomechanical properties could potentially be used to predict cardiac involvement in future studies.

Considering the widespread expression of *FBN1* in various ocular tissues, biomechanical changes in the cornea may reflect generalized alterations throughout the entire eye. The sclera, which has structural continuity with the cornea, both originating from the mesoderm, contains both elastin-containing and elastin-free microfibrillin. Previous studies have suggested that corneal biomechanics can serve as an indicator of the mechanical characteristics of the sclera and, to some extent, the lamina cribrosa. This relationship has been used to predict the progression of myopia and glaucoma.<sup>32,33</sup> Our previous research identified that the *FBN1* HI or DN (–Cys + CaB) patients also exhibited higher baseline AL and accelerated AL growth rate after lens surgery.<sup>17</sup> These findings align with the current study, which demonstrated that these mutation types are associated with reduced corneal stiffness in multivariate analysis. Therefore, this genotype–phenotype correlation underscores a genetic basis for using corneal biomechanical properties to predict AL

growth in pediatric patients after lens surgery in further studies.

Because patient demographics and biometric parameters also influence corneal biomechanical characteristics, this study further examined the impact of nongenotype factors. We found significant correlations between corneal biomechanics and variables such as gender, age, IOP, AL, CCT, and K, consistent with previous studies.<sup>34,35</sup> The literature presents conflicting findings regarding the relationship between EL severity and corneal biomechanical properties. For example, Jin et al.<sup>13</sup> revealed an increased corneal stiffness in MFS with severe EL, whereas Kara et al.<sup>25</sup> found the opposite. This study did not observe any significant correlation between EL severity and corneal stiffness. The zonules apply tensile forces to the eye wall against IOP, and their weakening or rupture could indirectly affect the eye's external dimensions and corneal sphericity.<sup>36</sup> However, this influence is complex, affected by factors such as the direction of lens tilt and the progressive nature of EL, and therefore requires further investigation. The indicators for corneal ectasia, including Corvis Biomechanical Index, BAD D, and TBI, were mainly associated with CCT, K, and corneal astigmatism, rather than *FBN1* genotype. This finding is reasonable, given that corneal ectasia is rare in cohorts patients with MFS.<sup>37</sup> In this study, although the PD, SSI, and DA ratios initially showed associations with the *FBN1* genotype, only the DA ratio maintained signif-

icant genotype–phenotype correlations after adjusting for confounding factors, independent of age or AL. This robust association underscores the potential of the DA ratio as a reliable biomarker for *FBN1*-related corneal biomechanical alterations. The DA ratio, which reflects intrinsic tissue properties through dynamic deformation analysis, is particularly sensitive to changes in extracellular matrix composition and microfibril structure—key features affected by *FBN1* mutations. Its independence from age and AL further enhances its clinical usefulness, making it a promising indicator for assessing corneal biomechanical integrity in *FBN1*-related connective tissue disorders. This finding aligns with previous research establishing the DA ratio as a valuable diagnostic parameter in keratoconus,<sup>38</sup> and our findings extend its application to *FBN1*-related disorders.

Several limitations should be considered when interpreting these results. First, corneal biomechanical properties were not measured routinely in the healthy and young patients who simultaneously had long AL, limiting the comparison between patients with MFS and controls to a relatively small sample size. However, this study prioritized investigating the inherent variations in corneal biomechanical properties among patients with MFS, offering a more practical approach to controlling confounding factors. In addition, the genotype classification used in this study was based mainly on DNA sequences and lacked validation at the RNA and protein levels. Further functional analysis of these mutations is needed to establish a more precise correlation between the effects of *FBN1* mutations and changes in corneal stiffness.

## CONCLUSIONS

The corneal biomechanical properties were associated significantly with the *FBN1* genotype. The CorVis ST technology presents a novel in vivo platform for assessing the impact of *FBN1* mutations, laying the groundwork for further investigation into the relationship between corneal biomechanics and ocular or systemic manifestations in patients with MFS. This study not only opens new avenues for research, but also offers promising directions worth exploring.

## Acknowledgments

The authors thank Yiyong Xian, Lingling Niu, and all the participants in this study.

Supported by National Natural Science Foundation of China (grant nos. 82401230, 82271068 and 82070943); Shanghai Municipal Commission of Health (grant no. 2024401591) and the Shanghai Science and Technology Commission (Scientific Innovation Action Plan, grant nos. 22Y11910400 and 20Y11911000).

**Author Contributions:** YJ, QH, and ZC were responsible for the research design of this article. QH, WJ, and YW collected the clinical data for patients with MFS. QH was responsible for statistical analyses. XS provided critical suggestions. YJ and YL supervised the whole project and has taken responsibility for the work. RZ contributed equally to this work. All authors in this study reviewed and revised the final manuscript.

**Data Availability Statement:** Data are available upon request.

**Disclosure:** Q.-Y. Huo, None; R.-Z. Zhang, None; W.-N. Jia, None; Y.-L. Wang, None; X. Shen, None; X.-Y. Chen, None;

T.-H. Chen, None; Y. Liu, None; L.-H. Song, None; X. Wang, None; Y. Lv, None; Z.-X. Chen, None; Y.-X. Jiang, None

## References

- Eckersley A, Mellody KT, Pilkington S. Structural and compositional diversity of fibrillin microfibrils in human tissues. *J Biol Chem*. 2018;293(14):5117–5133.
- Peeters S, De Kinderen P, Meester JAN. The fibrillinopathies: New insights with focus on the paradigm of opposing phenotypes for both *FBN1* and *FBN2*. *Hum Mutat*. 2022;43(7):815–831.
- Chen ZX, Jia WN, Jiang YX. Genotype-phenotype correlations of Marfan syndrome and related fibrillinopathies: Phenomenon and molecular relevance. *Front Genet*. 2022;13:943083.
- Arnaud P, Milleron O, Hanna N. Clinical relevance of genotype-phenotype correlations beyond vascular events in a cohort study of 1500 Marfan syndrome patients with *FBN1* pathogenic variants. *Genet Med*. 2021;23(7):1296–1304.
- Bonetti MI. Microfibrils: a cornerstone of extracellular matrix and a key to understand Marfan syndrome. *Ital J Anat Embryol*. 2009;114:201–224.
- Feneck EM, Lewis PN, Ralphs J. A comparative study of the elastic fibre system within the mouse and human cornea. *Exp Eye Res*. 2018;177:35–44.
- Chen J, Jing Q, Tang Y. Age differences in axial length, corneal curvature, and corneal astigmatism in Marfan syndrome with ectopia lentis. *J Ophthalmol*. 2018;2018:1436834.
- Zhang Y, Jin G, Young CA. Analysis of corneal astigmatism before surgery in Chinese congenital ectopia lentis patients. *Curr Eye Res*. 2018;43(8):972–976.
- Tack M, Kreps EO, De Zaeytjij J. Scheimpflug-based analysis of the reflectivity of the cornea in Marfan syndrome. *Transl Vis Sci Technol*. 2021;10(9):34.
- Chen J, Tang Y, Jing Q. Analysis of corneal spherical aberrations in Chinese bilateral ectopia lentis patients. *Front Med (Lausanne)*. 2021;8:736686.
- Liu MX, Zhu KY, Li DL. Corneal biomechanical characteristics in myopes and emmetropes measured by Corvis ST: a meta-analysis. *Am J Ophthalmol*. 2024;264:154–161.
- Loeys BL, Dietz HC, Braverman AC. The revised Ghent nosology for the Marfan syndrome. *J Med Genet*. 2010;47(7):476–485.
- Jin G, Zou M, Li L. Corneal biomechanics and their association with severity of lens dislocation in Marfan syndrome. *Int Ophthalmol*. 2024;44(1):148.
- Beene LC, Traboulsi EI, Seven I. Corneal deformation response and ocular geometry: a noninvasive diagnostic strategy in Marfan syndrome. *Am J Ophthalmol*. 2016;161:56–64.e51.
- Scheibenberger D, Frings A, Steinberg J. Ocular manifestation in Marfan syndrome: corneal biomechanical properties relate to increased systemic score points. *Graefes Arch Clin Exp Ophthalmol*. 2018;256(6):1159–1163.
- Kara N, Bozkurt E, Baz O. Corneal biomechanical properties and intraocular pressure measurement in Marfan patients. *J Cataract Refract Surg*. 2012;38(2):309–314.
- Chen Z-X, Jia W-N, Chen T-H. Genotype impacts axial length growth in pseudophakic eyes of Marfan syndrome. *Invest Ophthalmol Vis Sci*. 2023;64(10):28–28.
- Muñoz-Mosquera L, Steijns F, Audenaert T. Tailoring the American College of Medical Genetics and Genomics and the Association for Molecular Pathology guidelines for the interpretation of sequenced variants in the *FBN1* gene for Marfan syndrome: proposal for a disease-and gene-specific guideline. *Circ Genom Prec Med*. 2018;11(6):e002039.



19. Chen Z, Chen T, Zhang M. Fibrillin-1 gene mutations in a Chinese cohort with congenital ectopia lentis: spectrum and genotype–phenotype analysis. *Br J Ophthalmol*. 2022;106(12):1655–1661.
20. Meek KM, Knupp C, Lewis PN. Structural control of corneal transparency, refractive power and dynamics. *Eye*. 2024; doi:10.1038/s41433-024-02969-7. Online ahead of print.
21. Esporcatte LPG, Salomão MQ, Lopes BT. Biomechanics in keratoconus diagnosis. *Curr Eye Res*. 2023;48(2):130–136.
22. Izquierdo L, Gomez I, Moctezuma C. Biometric and corneal characteristics in Marfan syndrome with ectopia lentis. *J Fr Ophthalmol*. 2024;47(4):104096.
23. Feneck EM, Souza RB, Lewis PN. Developmental abnormalities in the cornea of a mouse model for Marfan syndrome. *Exp Eye Res*. 2020;194:108001.
24. Konradsen TR, Koivula A, Kugelberg M. Corneal curvature, pachymetry, and endothelial cell density in Marfan syndrome. *Acta Ophthalmol*. 2012;90(4):375–379.
25. Kara N, Bozkurt E, Baz O. Corneal biomechanical properties and intraocular pressure measurement in Marfan patients. *J Cataract Refract Surg*. 2012;38(2):309–314.
26. Chen ZX, Chen TH, Zhang M. Correlation between *FBN1* mutations and ocular features with ectopia lentis in the setting of Marfan syndrome and related fibrillinopathies. *Human Mutat*. 2021;42(12):1637–1647.
27. Wang Y, Lian Z, Zhou Y. Differential diagnosis of Marfan syndrome based on ocular biologic parameters. *Ann Transl Med*. 2020;8(21):1354.
28. Takeda N, Inuzuka R, Maemura S. Impact of pathogenic *FBN1* variant types on the progression of aortic disease in patients with Marfan syndrome. *Circ Genom Precis Med*. 2018;11(6):e002058.
29. Comeglio P, Johnson P, Arno G. The importance of mutation detection in Marfan syndrome and Marfan-related disorders: report of 193 *FBN1* mutations. *Human Mutat*. 2007;28(9):928–928.
30. Stengl R, Bors A, Ágg B. Optimising the mutation screening strategy in Marfan syndrome and identifying genotypes with more severe aortic involvement. *Orphanet J Rare Dis*. 2020;15:1–13.
31. Yadin DA, Robertson IB, McNaught-Davis J. Structure of the fibrillin-1 N-terminal domains suggests that heparan sulfate regulates the early stages of microfibril assembly. *Structure*. 2013;21(10):1743–1756.
32. Liu MX, Zhou M, Li DL. Corneal biomechanics in primary open angle glaucoma and ocular hypertension: a systematic review and meta-analysis. *J Glaucoma*. 2023;32(3):e24–e32.
33. Chu Z, Ren Q, Chen M. The relationship between axial length/corneal radius of curvature ratio and stress–strain index in myopic eyeballs: using Corvis ST tonometry. *Front Bioeng Biotechnol*. 2022;10:939129.
34. Narayanaswamy A, Chung RS, Wu R-Y. Determinants of corneal biomechanical properties in an adult Chinese population. *Ophthalmology*. 2011;118(7):1253–1259.
35. Strobbe E, Cellini M, Barbaresi U. Influence of age and gender on corneal biomechanical properties in a healthy Italian Population. *Cornea*. 2014;33(9):968–972.
36. Bassnett S. Zinn's zonule. *Prog Retina Eye Res*. 2021;82:100902.
37. Gehle P, Goergen B, Pilger D. Biometric and structural ocular manifestations of Marfan syndrome. *PloS One*. 2017;12(9):e0183370.
38. Vinciguerra R, Ambrósio R, Jr, Elsheikh A. Detection of keratoconus with a new biomechanical index. *J Refract Surg*. 2016;32(12):803–810.